Pseudorapidity Dependence of Particle Production and Elliptic Flow in Asymmetric Nuclear Collisions of $p+\mathrm{Al}$, $p+\mathrm{Au}$, $d+\mathrm{Au}$, and $^3\mathrm{He}+\mathrm{Au}$ at $\sqrt{s_{NN}}=200$ GeV

A. Adare,[13] C. Aidala,[41] N. N. Ajitanand,[57,*] Y. Akiba,[52,53,†] M. Alfred,[23] V. Andrieux,[41] K. Aoki,[31,52] N. Apadula,[28,58] H. Asano,[34,52] C. Ayuso,[41] B. Azmoun,[7] V. Babintsev,[24] M. Bai,[6] N. S. Bandara,[40] B. Bannier,[58] K. N. Barish,[8] S. Bathe,[5,53] A. Bazilevsky,[7] M. Beaumier,[8] S. Beckman,[13] R. Belmont,[13,41] A. Berdnikov,[55] Y. Berdnikov,[55] D. S. Blau,[33,44] M. Boer,[36] J. S. Bok,[46] K. Boyle,[53] M. L. Brooks,[36] J. Bryslawskyj,[5,8] V. Bumazhnov,[24] C. Butler,[21] S. Campbell,[14,28] V. Canoa Roman,[58] R. Cervantes,[58] C.-H. Chen,[53] C. Y. Chi,[14] M. Chiu,[7] I. J. Choi,[25] J. B. Choi,[10,*] T. Chujo,[61] Z. Citron,[63] M. Connors,[21,53] N. Cronin,[42,58] M. Csanád,[17] T. Csörgő,[18,64] T. W. Danley,[47] A. Datta,[45] M. S. Daugherity,[1] G. David,[7,16,58] K. DeBlasio,[45] K. Dehmelt,[58] A. Denisov,[24] A. Deshpande,[7,53,58] E. J. Desmond,[7] A. Dion,[58] P. B. Diss,[39] D. Dixit,[58] J. H. Do,[65] A. Drees,[58] K. A. Drees,[6] M. Dumancic,[63] J. M. Durham,[36] A. Durum,[24] T. Elder,[21] A. Enokizono,[52,54] H. En'yo,[52] S. Esumi,[61] B. Fadem,[42] W. Fan,[58] N. Feege,[58] D. E. Fields,[45] M. Finger,[9] M. Finger, Jr.,[9] S. L. Fokin,[33] J. E. Frantz,[47] A. Franz,[7] A. D. Frawley,[20] Y. Fukuda,[61] C. Gal,[58] P. Gallus,[15] P. Garg,[3,58] H. Ge,[58] F. Giordano,[25] A. Glenn,[35] Y. Goto,[52,53] N. Grau,[2] S. V. Greene,[62] M. Grosse Perdekamp,[25] T. Gunji,[12] H. Guragain,[21] T. Hachiya,[43,52,53] J. S. Haggerty,[7] K. I. Hahn,[19] H. Hamagaki,[12] H. F. Hamilton,[1] S. Y. Han,[19,52] J. Hanks,[58] S. Hasegawa,[29] T. O. S. Haseler,[21] K. Hashimoto,[52,54] X. He,[21] T. K. Hemmick,[58] J. C. Hill,[28] K. Hill,[13] A. Hodges,[21] R. S. Hollis,[8] K. Homma,[22] B. Hong,[32] T. Hoshino,[22] N. Hotvedt,[28] J. Huang,[7] S. Huang,[62] K. Imai,[29] J. Imrek,[16] M. Inaba,[61] A. Iordanova,[8] D. Isenhower,[1] Y. Ito,[43] D. Ivanishchev,[51] B. V. Jacak,[58] M. Jezghani,[21] Z. Ji,[58] J. Jia,[7,57] X. Jiang,[36] B. M. Johnson,[7,21] V. Jorjadze,[58] D. Jouan,[49] D. S. Jumper,[25] S. Kanda,[12] J. H. Kang,[65] D. Kapukchyan,[8] S. Karthas,[58] D. Kawall,[40] A. V. Kazantsev,[33] J. A. Key,[45] V. Khachatryan,[58] A. Khanzadeev,[51] C. Kim,[8,32] D. J. Kim,[30] E.-J. Kim,[10] G. W. Kim,[19] M. Kim,[52,56] M. H. Kim,[32] B. Kimelman,[42] D. Kincses,[17] E. Kistenev,[7] R. Kitamura,[12] J. Klatsky,[20] D. Kleinjan,[8] P. Kline,[58] T. Koblesky,[13] B. Komkov,[51] D. Kotov,[51,55] S. Kudo,[61] B. Kurgyis,[17] K. Kurita,[54] M. Kurosawa,[52,53] Y. Kwon,[65] R. Lacey,[57] J. G. Lajoie,[28] E. O. Lallow,[42] A. Lebedev,[28] S. Lee,[65] S. H. Lee,[28,58] M. J. Leitch,[36] Y. H. Leung,[58] N. A. Lewis,[41] X. Li,[11] X. Li,[36] S. H. Lim,[36,65] L. D. Liu,[50] M. X. Liu,[36] V.-R. Loggins,[25] S. Lökös,[17,18] K. Lovasz,[16] D. Lynch,[7] T. Majoros,[16] Y. I. Makdisi,[6] M. Makek,[66] M. Malaev,[51] A. Manion,[58] V. I. Manko,[33] E. Mannel,[7] H. Masuda,[54] M. McCumber,[36] P. L. McGaughey,[36] D. McGlinchey,[13,36] C. McKinney,[25] A. Meles,[46] M. Mendoza,[8] W. J. Metzger,[18] A. C. Mignerey,[39] D. E. Mihalik,[58] A. Milov,[63] D. K. Mishra,[4] J. T. Mitchell,[7] I. Mitrankov,[55] G. Mitsuka,[31,52,53] S. Miyasaka,[52,60] S. Mizuno,[52,61] A. K. Mohanty,[4] P. Montuenga,[25] T. Moon,[65] D. P. Morrison,[7] S. I. Morrow,[62] T. V. Moukhanova,[33] T. Murakami,[34,52] J. Murata,[52,54] A. Mwai,[57] K. Nagai,[60] K. Nagashima,[22,52] T. Nagashima,[54] J. L. Nagle,[13] M. I. Nagy,[17] I. Nakagawa,[52,53] H. Nakagomi,[52,61] K. Nakano,[52,60] C. Nattrass,[59] P. K. Netrakanti,[4] T. Niida,[61] S. Nishimura,[12] R. Nishitani,[43] R. Nouicer,[7,53] T. Novák,[18,64] N. Novitzky,[30,58] R. Novotny,[15] A. S. Nyanin,[33] E. O'Brien,[7] C. A. Ogilvie,[28] J. D. Orjuela Koop,[13] J. D. Osborn,[41] A. Oskarsson,[37] G. J. Ottino,[45] K. Ozawa,[31,61] R. Pak,[7] V. Pantuev,[26] V. Papavassiliou,[46] J. S. Park,[56] S. Park,[52,56,58] S. F. Pate,[46] M. Patel,[28] J.-C. Peng,[25] W. Peng,[62] D. V. Perepelitsa,[7,13] G. D. N. Perera,[46] D. Yu. Peressounko,[33] C. E. PerezLara,[58] J. Perry,[28] R. Petti,[7,58] M. Phipps,[7,25] C. Pinkenburg,[7] R. Pinson,[1] R. P. Pisani,[7] A. Pun,[47] M. L. Purschke,[7] P. V. Radzevich,[55] J. Rak,[30] B. J. Ramson,[41] I. Ravinovich,[63] K. F. Read,[48,59] D. Reynolds,[57] V. Riabov,[44,51] Y. Riabov,[51,55] D. Richford,[5] T. Rinn,[28] S. D. Rolnick,[8] M. Rosati,[28] Z. Rowan,[5] J. G. Rubin,[41] J. Runchey,[28] A. S. Safonov,[55] B. Sahlmueller,[58] N. Saito,[31] T. Sakaguchi,[7] H. Sako,[29] V. Samsonov,[44,51] M. Sarsour,[21] K. Sato,[61] S. Sato,[29] B. Schaefer,[62] B. K. Schmoll,[59] K. Sedgwick,[8] R. Seidl,[52,53] A. Sen,[28,59] R. Seto,[8] P. Sett,[4] A. Sexton,[39] D. Sharma,[58] I. Shein,[24] T.-A. Shibata,[52,60] K. Shigaki,[22] M. Shimomura,[28,43] T. Shioya,[61] P. Shukla,[4] A. Sickles,[7,25] C. L. Silva,[36] D. Silvermyr,[37,48] B. K. Singh,[3] C. P. Singh,[3] V. Singh,[3] M. J. Skoby,[41] M. Slunečka,[9] K. L. Smith,[20] M. Snowball,[36] R. A. Soltz,[35] W. E. Sondheim,[36] S. P. Sorensen,[59] I. V. Sourikova,[7] P. W. Stankus,[48] M. Stepanov,[40,*] S. P. Stoll,[7] T. Sugitate,[22] A. Sukhanov,[7] T. Sumita,[52] J. Sun,[58] Z. Sun,[16] S. Suzuki,[43] S. Syed,[21] J. Sziklai,[64] A. Takeda,[43] A. Taketani,[52,53] K. Tanida,[29,53,56] M. J. Tannenbaum,[7] S. Tarafdar,[62,63] A. Taranenko,[44,57] G. Tarnai,[16] R. Tieulent,[21,38] A. Timilsina,[28] T. Todoroki,[52,53,61] M. Tomášek,[15] C. L. Towell,[1] R. Towell,[1] R. S. Towell,[1] I. Tserruya,[63] Y. Ueda,[22] B. Ujvari,[16] H. W. van Hecke,[36] S. Vazquez-Carson,[13] J. Velkovska,[62] M. Virius,[15] V. Vrba,[15,27] N. Vukman,[66] X. R. Wang,[46,53] Z. Wang,[5] Y. Watanabe,[52,53] Y. S. Watanabe,[12,31] F. Wei,[46] A. S. White,[41] C. P. Wong,[21] C. L. Woody,[7]

M. Wysocki,[48] B. Xia,[47] C. Xu,[46] Q. Xu,[62] L. Xue,[21] S. Yalcin,[58] Y. L. Yamaguchi,[12,53,58] H. Yamamoto,[61] A. Yanovich,[24] P. Yin,[13] J. H. Yoo,[32,53] I. Yoon,[56] H. Yu,[46,50] I. E. Yushmanov,[33] W. A. Zajc,[14] A. Zelenski,[6] S. Zharko,[55] S. Zhou,[11] and L. Zou[8]

(PHENIX Collaboration)

[1]*Abilene Christian University, Abilene, Texas 79699, USA*
[2]*Department of Physics, Augustana University, Sioux Falls, South Dakota 57197, USA*
[3]*Department of Physics, Banaras Hindu University, Varanasi 221005, India*
[4]*Bhabha Atomic Research Centre, Bombay 400 085, India*
[5]*Baruch College, City University of New York, New York, New York, 10010 USA*
[6]*Collider-Accelerator Department, Brookhaven National Laboratory, Upton, New York 11973-5000, USA*
[7]*Physics Department, Brookhaven National Laboratory, Upton, New York 11973-5000, USA*
[8]*University of California-Riverside, Riverside, California 92521, USA*
[9]*Charles University, Ovocný trh 5, Praha 1, 116 36 Prague, Czech Republic*
[10]*Chonbuk National University, Jeonju 561-756, Korea*
[11]*Science and Technology on Nuclear Data Laboratory, China Institute of Atomic Energy, Beijing 102413, People's Republic of China*
[12]*Center for Nuclear Study, Graduate School of Science, University of Tokyo, 7-3-1 Hongo, Bunkyo, Tokyo 113-0033, Japan*
[13]*University of Colorado, Boulder, Colorado 80309, USA*
[14]*Columbia University, New York, New York 10027 and Nevis Laboratories, Irvington, New York 10533, USA*
[15]*Czech Technical University, Zikova 4, 166 36 Prague 6, Czech Republic*
[16]*Debrecen University, H-4010 Debrecen, Egyetem tér 1, Hungary*
[17]*ELTE, Eötvös Loránd University, H-1117 Budapest, Pázmány P. s. 1/A, Hungary*
[18]*Eszterházy Károly University, Károly Róbert Campus, H-3200 Gyöngyös, Mátrai út 36, Hungary*
[19]*Ewha Womans University, Seoul 120-750, Korea*
[20]*Florida State University, Tallahassee, Florida 32306, USA*
[21]*Georgia State University, Atlanta, Georgia 30303, USA*
[22]*Hiroshima University, Kagamiyama, Higashi-Hiroshima 739-8526, Japan*
[23]*Department of Physics and Astronomy, Howard University, Washington, DC 20059, USA*
[24]*IHEP Protvino, State Research Center of Russian Federation, Institute for High Energy Physics, Protvino, 142281, Russia*
[25]*University of Illinois at Urbana-Champaign, Urbana, Illinois 61801, USA*
[26]*Institute for Nuclear Research of the Russian Academy of Sciences, prospekt 60-letiya Oktyabrya 7a, Moscow 117312, Russia*
[27]*Institute of Physics, Academy of Sciences of the Czech Republic, Na Slovance 2, 182 21 Prague 8, Czech Republic*
[28]*Iowa State University, Ames, Iowa 50011, USA*
[29]*Advanced Science Research Center, Japan Atomic Energy Agency, 2-4 Shirakata Shirane, Tokai-mura, Naka-gun, Ibaraki-ken 319-1195, Japan*
[30]*Helsinki Institute of Physics and University of Jyväskylä, P.O. Box 35, FI-40014 Jyväskylä, Finland*
[31]*KEK, High Energy Accelerator Research Organization, Tsukuba, Ibaraki 305-0801, Japan*
[32]*Korea University, Seoul 136-701, Korea*
[33]*National Research Center "Kurchatov Institute," Moscow 123098, Russia*
[34]*Kyoto University, Kyoto 606-8502, Japan*
[35]*Lawrence Livermore National Laboratory, Livermore, California 94550, USA*
[36]*Los Alamos National Laboratory, Los Alamos, New Mexico 87545, USA*
[37]*Department of Physics, Lund University, Box 118, SE-221 00 Lund, Sweden*
[38]*IPNL, CNRS/IN2P3, Université Lyon, Université Lyon 1, F-69622, Villeurbanne, France*
[39]*University of Maryland, College Park, Maryland 20742, USA*
[40]*Department of Physics, University of Massachusetts, Amherst, Massachusetts 01003-9337, USA*
[41]*Department of Physics, University of Michigan, Ann Arbor, Michigan 48109-1040, USA*
[42]*Muhlenberg College, Allentown, Pennsylvania 18104-5586, USA*
[43]*Nara Women's University, Kita-uoya Nishi-machi Nara 630-8506, Japan*
[44]*National Research Nuclear University, MEPhI, Moscow Engineering Physics Institute, Moscow 115409, Russia*
[45]*University of New Mexico, Albuquerque, New Mexico 87131, USA*
[46]*New Mexico State University, Las Cruces, New Mexico 88003, USA*
[47]*Department of Physics and Astronomy, Ohio University, Athens, Ohio 45701, USA*
[48]*Oak Ridge National Laboratory, Oak Ridge, Tennessee 37831, USA*
[49]*IPN-Orsay, Université Paris-Sud, CNRS/IN2P3, Université Paris-Saclay, BP1, F-91406 Orsay, France*
[50]*Peking University, Beijing 100871, People's Republic of China*
[51]*PNPI, Petersburg Nuclear Physics Institute, Gatchina, Leningrad region 188300, Russia*

[52]RIKEN Nishina Center for Accelerator-Based Science, Wako, Saitama 351-0198, Japan
[53]RIKEN BNL Research Center, Brookhaven National Laboratory, Upton, New York 11973-5000, USA
[54]Physics Department, Rikkyo University, 3-34-1 Nishi-Ikebukuro, Toshima, Tokyo 171-8501, Japan
[55]Saint Petersburg State Polytechnic University, St. Petersburg, 195251 Russia
[56]Department of Physics and Astronomy, Seoul National University, Seoul 151-742, Korea
[57]Chemistry Department, Stony Brook University, SUNY, Stony Brook, New York 11794-3400, USA
[58]Department of Physics and Astronomy, Stony Brook University, SUNY, Stony Brook, New York 11794-3800, USA
[59]University of Tennessee, Knoxville, Tennessee 37996, USA
[60]Department of Physics, Tokyo Institute of Technology, Oh-okayama, Meguro, Tokyo 152-8551, Japan
[61]Tomonaga Center for the History of the Universe, University of Tsukuba, Tsukuba, Ibaraki 305, Japan
[62]Vanderbilt University, Nashville, Tennessee 37235, USA
[63]Weizmann Institute, Rehovot 76100, Israel
[64]Institute for Particle and Nuclear Physics, Wigner Research Centre for Physics, Hungarian Academy of Sciences (Wigner RCP, RMKI) H-1525 Budapest 114, P.O. Box 49, Budapest, Hungary
[65]Yonsei University, IPAP, Seoul 120-749, Korea
[66]Department of Physics, Faculty of Science, University of Zagreb, Bijenička c. 32 HR-10002 Zagreb, Croatia

(Received 1 August 2018; revised manuscript received 12 October 2018; published 29 November 2018)

Asymmetric nuclear collisions of $p+\mathrm{Al}$, $p+\mathrm{Au}$, $d+\mathrm{Au}$, and $^3\mathrm{He}+\mathrm{Au}$ at $\sqrt{s_{NN}}=200$ GeV provide an excellent laboratory for understanding particle production, as well as exploring interactions among these particles after their initial creation in the collision. We present measurements of charged hadron production $dN_{\mathrm{ch}}/d\eta$ in all such collision systems over a broad pseudorapidity range and as a function of collision multiplicity. A simple wounded quark model is remarkably successful at describing the full data set. We also measure the elliptic flow v_2 over a similarly broad pseudorapidity range. These measurements provide key constraints on models of particle emission and their translation into flow.

DOI: 10.1103/PhysRevLett.121.222301

Asymmetric nuclear collisions with a light projectile nucleus striking a heavier target nucleus have proven to be an excellent testing ground for particle production models and the longitudinal dynamics following the initial collision—for an early review, see Ref. [1]. Many calculations have successfully described the longitudinal (or rapidity) distribution of produced particles in proton-nucleus ($p+A$) collisions via the fragmentation of color strings and with counting rules based on the number of "wounded" or struck nucleons or quarks in the projectile and target. Recently, a proposal for testing the wounded-quark model [2] was put forth that specifically called for the measurement of $dN_{\mathrm{ch}}/d\eta$ over a broad range of pseudorapidity in $p+\mathrm{Au}$, $d+\mathrm{Au}$, and $^3\mathrm{He}+\mathrm{Au}$ collisions [3]. Fully three-dimensional hydrodynamical models also require input on the longitudinal distribution of initial deposited energy and gradients thereof [4]. Once the initial partons or fluid elements are populated, the models evolve the system dynamically. Measurements of elliptic flow as a function of pseudorapidity provide constraints on the longitudinal dynamics of the evolution.

As the incoming hadrons or nuclei break up, the rapidity distribution of liberated partons may be determined by the longitudinal parton distribution functions [5,6] or via a universal color field breakup for each struck nucleon or quark [7]. For that reason, calculations based on Monte Carlo Glauber models have been developed to calculate the number of struck nucleons and struck quarks (see, e.g., Refs. [8–10]). The PHOBOS Collaboration has previously published charged hadron $dN_{\mathrm{ch}}/d\eta$ measurements over $|\eta|<5.4$ in $d+\mathrm{Au}$ collisions at $\sqrt{s_{NN}}=200$ GeV [11]. PHENIX has also published $dN_{\mathrm{ch}}/d\eta$ measurements in high-multiplicity $d+\mathrm{Au}$ collisions at $\sqrt{s_{NN}}=200$, 62, 39, and 19.6 GeV [12]. The wounded-quark model has been constrained by the $d+\mathrm{Au}$ data and found to be in reasonable agreement with the centrality dependence, while the wounded-nucleon model cannot describe the data [3]. A crucial test of the wounded-quark model is to see if it is universal across different colliding systems. Additional measurements in light and heavy systems at the Relativistic Heavy Ion Collider (RHIC) and the Large Hadron Collider (LHC) can also be tested in this context—see, e.g., different geometry tests in Refs. [13–15].

In $\mathrm{Au}+\mathrm{Au}$ and $\mathrm{Pb}+\mathrm{Pb}$ collisions at RHIC and the LHC, the created medium is well described by low-viscosity hydrodynamics [16,17]. A host of recent experimental observations indicate that hydrodynamics may also be applicable to the asymmetric collisions of small nuclear systems, e.g., $p+A$, $d+\mathrm{Au}$, $^3\mathrm{He}+\mathrm{Au}$, and perhaps even $p+p$ (for a recent review, see Ref. [18]). In heavy ion collisions, the hydrodynamical flow of the medium is characterized via a Fourier decomposition of

the final hadron momentum anisotropy in the direction transverse to the incoming beam directions [19] as

$$\frac{dN}{d\phi} \propto 1 + \sum_n 2v_n \cos\left[n(\phi - \psi_n)\right], \tag{1}$$

where n is the harmonic number, ϕ is the particle azimuthal angle, ψ_n is the nth-order symmetry axis, and v_n is the Fourier coefficient, with v_2 referred to as the elliptic flow. The pseudorapidity dependence of v_2 has been measured in Au + Au and Pb + Pb collisions at RHIC and the LHC, and the elliptic flow is smaller in regions with a smaller final hadron $dN_{\rm ch}/d\eta$—see, e.g., Refs. [20,21]. The data have been interpreted in terms of hydrodynamics and imply a shear viscosity to entropy density, η/s, that is temperature dependent [22]. Similar measurements in small nuclear collisions of different sizes are a key test for how local rapidity density relates to hydrodynamical evolution into flow.

In this Letter, we present a comprehensive set of measurements of $dN_{\rm ch}/d\eta$ and elliptic flow v_2 over a broad pseudorapidity range in p + Al, p + Au, d + Au, and ^{3}He + Au collisions at $\sqrt{s_{NN}} = 200$ GeV. The data sets analyzed were recorded in 2014 for ^{3}He + Au, in 2015 for p + Al and p + Au, and in 2016 for d + Au. All data sets were recorded with a minimum-bias trigger that required at least one hit in each of the PHENIX beam-beam counters (BBCs). The BBC is composed of two detectors, each containing 64 quartz radiators read out with photomultiplier tubes [23]. The BBC covers positive and negative pseudorapidity $3.1 < |\eta| < 3.9$. Following the procedure from Ref. [24], the minimum-bias trigger is determined to fire on $88 \pm 4\%$, $88 \pm 4\%$, $84 \pm 3\%$, and $72 \pm 4\%$ of the total inelastic cross section of 2.30, 2.26, 1.76, 0.54 barns for ^{3}He + Au, d + Au, p + Au, and p + Al, respectively. The $dN_{\rm ch}/d\eta$ analysis has negligible statistical uncertainties, and thus a subset of runs with the most stable detector configuration are utilized, and the run-to-run variation is used in the determination of systematic uncertainties. For the elliptic flow v_2 analysis in high-multiplicity events, also referred to as central events, an additional trigger was used that required the number of fired BBC tubes to be above a set number, roughly corresponding to the 0%–5% highest-multiplicity events.

The characterization of the different collision systems and centralities follows the procedure detailed in Ref. [24]. The multiplicity class is selected by the total charge in the BBC covering negative pseudorapidity—i.e., in the Al- or Au-going direction. The total charge is found to scale with the total number of struck nucleons from the Al or Au nucleus folded with a negative binomial distribution, representing the fluctuations in the number of particles produced and measured by the BBC. The 5% most central events have an average number of participating nucleons of 5.1 ± 0.3, 10.7 ± 0.6, 17.8 ± 1.2, and 25.0 ± 1.6 for p + Al, p + Au, d + Au, and ^{3}He + Au, respectively.

Charged hadrons are reconstructed at midrapidity $|\eta| < 0.35$ with a combination of drift chambers and pad chambers [25]. Midrapidity tracks have their momentum reconstructed via their bend in a magnetic field and are efficiently measured for $p_T > 0.2$ GeV/c. At backward $-3.0 < \eta < -1.0$ and forward $1.0 < \eta < 3.0$ rapidity, the forward-silicon-vertex detector (FVTX) measures the traversal of charged tracks in four detector layers, as detailed in Ref. [26]. FVTX tracks are efficiently measured for $p_T > 0.3$ GeV/c, but with no momentum information, because the silicon strips are oriented lengthwise along the magnetic-field bend direction.

For the $dN_{\rm ch}/d\eta$ results, the absolute acceptance and efficiency for track reconstruction can be determined with the PHENIX GEANT-3 Monte Carlo simulation. However, in the last years of data taking, the PHENIX experiment had increasingly significant dead regions and run-to-run variations that became challenging to fully account for. Thus, we determine the acceptance and efficiency for a given running period in a control data set by taking the ratio $R(\eta)$ of published PHOBOS $dN_{\rm ch}/d\eta$ to the PHENIX raw $dN_{\rm ch}/d\eta$ as a function of pseudorapidity. The control PHOBOS data sets are Au + Au in 2014 [27], p + p in 2015 [27], and d + Au in 2016 [11], all at $\sqrt{s_{NN}} = 200$ GeV. This "bootstrapping" procedure is described in detail in Ref. [12]. Sources of systematic uncertainty come from varying the track selection cuts, run-to-run variations, and considering high- and low-luminosity running periods with different double-interaction contributions. We also find good agreement within uncertainties by comparing results in the FVTX with an absolute acceptance and efficiency calculation and the "bootstrapped" results.

The determination of hadron yields in centrality bins has a known bias effect (see Ref. [24]). In p + p collisions, inelastic events fire the BBC trigger $55 \pm 5\%$ of the time, while in events with a π^0 or charged hadron at midrapidity, that percentage is larger, $79 \pm 2\%$. This increased trigger efficiency is correlated with a 1.55 times larger BBC multiplicity. This effect results from the diffractive portion of the p + p inelastic cross section disfavoring midrapidity particle production. This bias has been confirmed for midrapidity hadron production down to $p_T \approx 0.5$ GeV/c [28] and for J/ψ measured in the PHENIX muons' arms [29], and thus we expect that this bias affects all charged hadrons over the pseudorapidity range studied here. We remove this bias via correction factors that are calculated following the procedure detailed in Ref. [24]. The bias corrections are largest in the smallest system and range from 0.75 ± 0.01 for central 0%–5% p + Al to 0.91 ± 0.01 for central 0%–5% ^{3}He + Au. We apply these bias correction factors to all our $dN_{\rm ch}/d\eta$ results.

Figure 1 shows the $dN_{\rm ch}/d\eta$ results for p + Al, p + Au, d + Au, and ^{3}He + Au at $\sqrt{s_{NN}} = 200$ GeV for the 5%

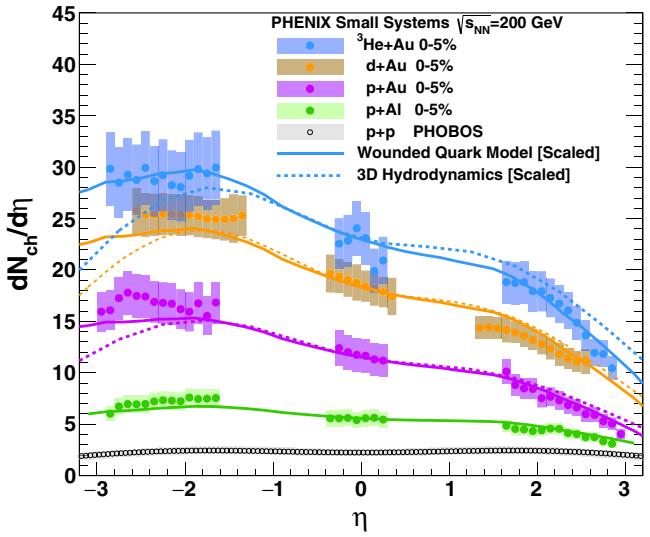

FIG. 1. Charged hadron $dN_{\rm ch}/d\eta$ as a function of pseudorapidity in high-multiplicity 0%–5% central ^{3}He + Au, d + Au, p + Au, and p + Al collisions at $\sqrt{s_{NN}} = 200$ GeV. Also shown are results in inelastic $p + p$ collisions at $\sqrt{s_{NN}} = 200$ GeV as measured by the PHOBOS Collaboration [27]. Predictions from the wounded-quark [3] and hydrodynamical [4] models are shown. The calculations have an overall normalization factor (S) to best match the data. These factors are $S = 0.88$, 0.93, 0.85, and 0.77 for the wounded-quark model for p + Al, p + Au, d + Au, and ^{3}He + Au, respectively; and $S = 0.81$, 0.96, and 0.75 for the hydrodynamical model for p + Au, d + Au, and ^{3}He + Au, respectively.

highest-multiplicity events. Statistical uncertainties are negligible, and systematic uncertainties are shown as boxes around the points. The systematic uncertainties are point-to-point correlated and can in principle move the backward, mid-, and forward rapidity points separately, because they are measured in different detectors. Also shown are the yields in inelastic $p + p$ collisions at $\sqrt{s_{NN}} = 200$ GeV as measured by the PHOBOS Collaboration [27]. The full set of multiplicity-selected results for the four asymmetric nuclear collision systems are shown in Fig. 2.

The results are compared to predictions from the wounded-quark model. Within the wounded-quark model, each wounded quark is posited to yield hadrons following a common emission function $F(\eta)$ [3]. $F(\eta)$ is constrained by d + Au collision data, and the model then predicts $dN_{\rm ch}/d\eta$ for all collision centralities and systems. The calculations are normalized, with factors listed in the Fig. 1 caption, to best match the data integrated over pseudorapidity, because the exact normalization can be influenced by modest differences in the centrality selection, and thus the mean number of wounded quarks. Within the systematic uncertainties on the experimental measurements, the model provides a good description of the complete data set across collision systems and centrality classes. The results are also compared in Fig. 1 with a hydrodynamical calculation [4] for 0%–5% central collisions. The calculation includes Monte Carlo Glauber initial conditions with longitudinal entropy distributions [30], (3 + 1)D viscous hydrodynamics [31] with $\eta/s = 1/4\pi$, and temperature-dependent bulk viscosity, followed by statistical hadronization. Again, the calculations are normalized to the data with factors listed in the caption. The agreement in this case is also good within systematic uncertainties, except for a more significant drop in particle yield in the calculation at the most backward rapidity region $-3.0 < \eta \lesssim -2.0$.

Midrapidity $dN_{\rm ch}/d\eta$ per participating quark pair, $N_{qp}/2$, scales as a function of the number of participating quarks from d + Au and ^{3}He + Au collisions [15]. The previously reported results [15] were not corrected for the modest bias previously discussed. Figure 3 shows the results testing this scaling for all small collision systems, each with the bias correction factors applied. Within the systematic uncertainties, all systems at all centralities follow a common scaling for midrapidity particle production.

In d + Au collisions, the elliptic flow v_2 was observed to have a similar pseudorapidity dependence to the particle yield $dN_{\rm ch}/d\eta$ [12]. For the other systems, we have followed the same procedure for measuring elliptic flow v_2 using the event-plane method, where the event plane is

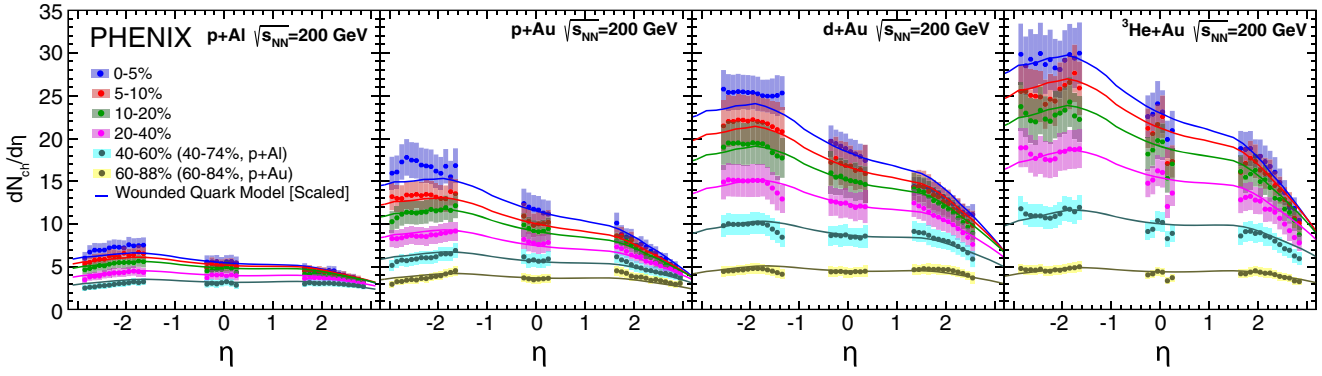

FIG. 2. Charged hadron $dN_{\rm ch}/d\eta$ as a function of pseudorapidity in various multiplicity classes of p + Al, p + Au, d + Au, and ^{3}He + Au collisions at $\sqrt{s_{NN}} = 200$ GeV. Predictions from the wounded-quark model [3] are shown.

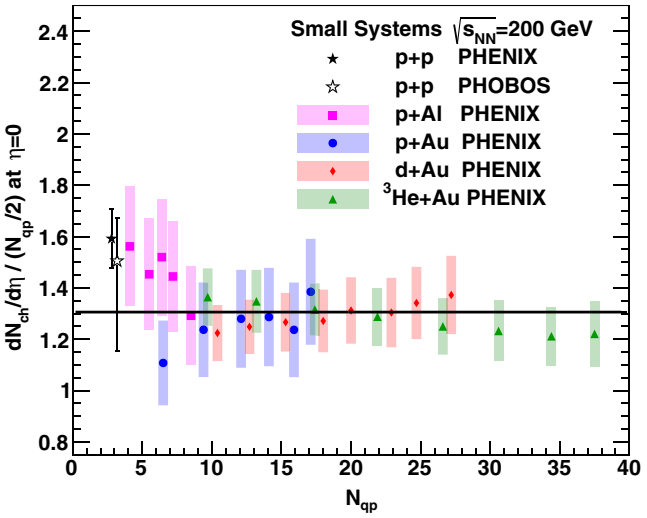

FIG. 3. Midrapidity charged hadron $dN_{\rm ch}/d\eta$ per participating quark pair ($N_{qp}/2$) as a function of the number of participating quarks (N_{qp}). Results are shown for $p+{\rm Al}$, $p+{\rm Au}$, $d+{\rm Au}$, and $^3{\rm He}+{\rm Au}$ collisions in various multiplicity classes. Also shown are previously published results in $p+p$ collisions from PHENIX [15] and PHOBOS [27]. The line is the best fit to all the data to a constant level.

defined by the Al- or Au-going BBC covering $-3.9 < \eta < -3.1$. The results are corrected using AMPT [32] and a GEANT-3 simulation of the detector to correspond to v_2 integrated over hadrons at all p_T's within each pseudorapidity bin. Systematic uncertainties are determined by varying the track selection cuts, collision z-vertex cuts, and AMPT input parameters.

Figure 4 shows the elliptic flow v_2 as a function of pseudorapidity in 0%–5% central $p+{\rm Al}$, $p+{\rm Au}$, $d+{\rm Au}$, and $^3{\rm He}+{\rm Au}$ collisions at $\sqrt{s_{NN}} = 200$ GeV. The experimental data have an increasing flow coefficient at forward rapidity when going from the smallest system and smallest particle production $p+{\rm Al}$ to the largest $^3{\rm He}+{\rm Au}$. These trends are consistent with arising from the combined influence of initial geometry and particle multiplicity [33]. The v_2 also increases towards backward rapidity for each collision system. For the lowest-multiplicity systems, $p+{\rm Al}$ and $p+{\rm Au}$, there is a sharp enhancement in the v_2 for $\eta \lesssim -2.0$ that is more pronounced in $p+{\rm Al}$. This feature may be due to the nonflow contribution of short-range correlations, because this is the pseudorapidity range that is within one unit of the BBC used for determining the event plane.

The data are compared with the same hydrodynamical model [4] that gave a reasonable description of the $dN_{\rm ch}/d\eta$. There is good qualitative agreement with the system and pseudorapidity dependence of v_2, and good quantitative agreement of its pseudorapidity dependence in $p+{\rm Au}$ and $d+{\rm Au}$. The only feature not qualitatively described is the enhancement at backward rapidity. This enhancement is the strongest in $p+{\rm Al}$, weaker but still pronounced in $p+{\rm Au}$, and rather weak in $d+{\rm Au}$. The strength of this enhancement trends inversely with the $dN_{\rm ch}/d\eta$, lending additional evidence that this is due to nonflow influences not incorporated in the hydrodynamical model. In $^3{\rm He}+{\rm Au}$ collisions, the hydrodynamical model overpredicts the forward rapidity ($\eta > 1$) v_2 by more than 50% and qualitatively has the feature of a weaker forward or backward asymmetry than what is present in the data. Note that the model overpredicts the $^3{\rm He}+{\rm Au}$ $dN_{\rm ch}/d\eta$ by approximately 25% (but is scaled to fit the data in Fig. 1), which may help explain the overpredicted v_2.

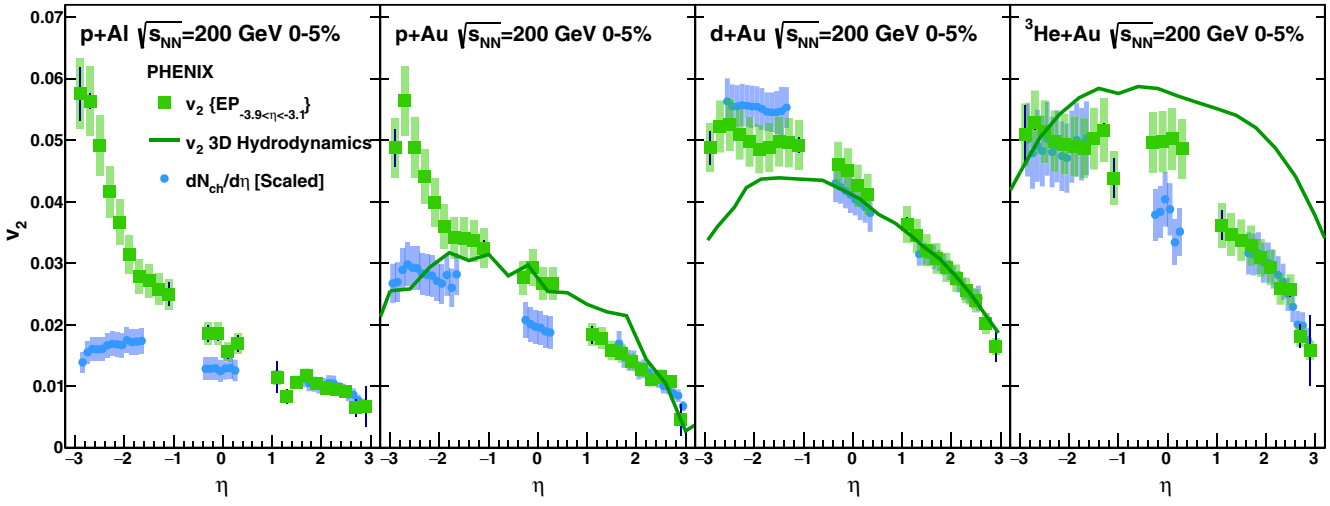

FIG. 4. Elliptic flow v_2 as a function of pseudorapidity in high-multiplicity 0%–5% central $p+{\rm Al}$, $p+{\rm Au}$, $d+{\rm Au}$, and $^3{\rm He}+{\rm Au}$ collisions at $\sqrt{s_{NN}} = 200$ GeV. Also shown are predictions from the hydrodynamical model [4]. Lastly, the measured $dN_{\rm ch}/d\eta$ results are shown scaled to match the v_2 at forward rapidity for shape comparison with the elliptic flow coefficients.

In Fig. 4, we also scale $dN_{\rm ch}/d\eta$ to match the v_2 at forward rapidity to compare the shape of the distributions. Although a larger local particle density $dN_{\rm ch}/d\eta$ is correlated with more elliptic flow, the scaling observed in $d+{\rm Au}$ appears to be only approximate when viewed in the context of all collision systems. It is notable that although not shown in Fig. 4, hydrodynamical model calculations [4] also do not exhibit an exact scaling relation $v_2 \propto dN_{\rm ch}/d\eta$.

We have presented a comprehensive set of measurements of particle production $dN_{\rm ch}/d\eta$ and elliptic flow v_2 over a broad pseudorapidity range for a suite of asymmetric nuclear collisions $p+{\rm Al}$, $p+{\rm Au}$, $d+{\rm Au}$, and $^3{\rm He}+{\rm Au}$ at $\sqrt{s_{NN}} = 200$ GeV. The particle production is remarkably well described in the context of the wounded-quark model [3]. A three-dimensional hydrodynamical model qualitatively describes the particle production and elliptic flow in high-multiplicity events in all collision systems. However, it overpredicts the overall $dN_{\rm ch}/d\eta$ and forward rapidity v_2 in $^3{\rm He}+{\rm Au}$ collisions. These data provide an important constraint on models of the longitudinal dynamics in these asymmetric collisions.

We thank the staff of the Collider-Accelerator and Physics Departments at Brookhaven National Laboratory and the staff of the other PHENIX participating institutions for their vital contributions. We thank Adam Bzdak and Piotr Bożek for providing theoretical calculations for the suite of collision systems and centralities from the wounded-quark model and hydrodynamical model, respectively. We acknowledge support from the Office of Nuclear Physics in the Office of Science of the Department of Energy, the National Science Foundation, the Abilene Christian University Research Council, the Research Foundation of SUNY, and the Dean of the College of Arts and Sciences, Vanderbilt University (U.S.); from the Ministry of Education, Culture, Sports, Science, and Technology and the Japan Society for the Promotion of Science (Japan); from the Conselho Nacional de Desenvolvimento Científico e Tecnológico and Fundação de Amparo à Pesquisa do Estado de São Paulo (Brazil); from the Natural Science Foundation of China (People's Republic of China); from the Croatian Science Foundation and Ministry of Science and Education (Croatia); from the Ministry of Education, Youth, and Sports (Czech Republic); from the Centre National de la Recherche Scientifique, Commissariat à l'Énergie Atomique, and Institut National de Physique Nucléaire et de Physique des Particules (France); from Bundesministerium für Bildung und Forschung, Deutscher Akademischer Austausch Dienst, and Alexander von Humboldt Stiftung (Germany); from the J. Bolyai Research Scholarship, EFOP, the New National Excellence Program (ÚNKP), NKFIH, and OTKA (Hungary); from the Department of Atomic Energy and Department of Science and Technology (India); from the Israel Science Foundation (Israel); from the Basic Science Research Program through NRF of the Ministry of Education (Korea); from the Physics Department, Lahore University of Management Sciences (Pakistan); from the Ministry of Education and Science, Russian Academy of Sciences, Federal Agency of Atomic Energy (Russia); from the VR and Wallenberg Foundation (Sweden); and from the U.S. Civilian Research and Development Foundation for the Independent States of the Former Soviet Union, the Hungarian American Enterprise Scholarship Fund, the US-Hungarian Fulbright Foundation, and the US-Israel Binational Science Foundation.

[*] Deceased.
[†] PHENIX Spokesperson.
akiba@rcf.rhic.bnl.gov

[1] W. Busza, Review of experimental data on hadron-nucleus collisions at high-energies, Acta Phys. Pol. B **8**, 333 (1977).
[2] S. Eremin and S. Voloshin, Nucleon participants or quark participants? Phys. Rev. C **67**, 064905 (2003).
[3] M. Barej, A. Bzdak, and P. Gutowski, Wounded-quark emission function at the top energy available at the BNL relativistic heavy ion collider, Phys. Rev. C **97**, 034901 (2018).
[4] P. Bozek and W. Broniowski, Collective flow in ultra-relativistic $^3{\rm He}+{\rm Au}$ collisions, Phys. Lett. B **739**, 308 (2014).
[5] J. Benecke, T. T. Chou, C. N. Yang, and E. Yen, Hypothesis of limiting fragmentation in high-energy collisions, Phys. Rev. **188**, 2159 (1969).
[6] F. Gelis, A. M. Stasto, and R. Venugopalan, Limiting fragmentation in hadron-hadron collisions at high energies, Eur. Phys. J. C **48**, 489 (2006).
[7] P. Bozek, W. Broniowski, and M. Rybczynski, Wounded quarks in $A+A$, $p+A$, and $p+p$ collisions, Phys. Rev. C **94**, 014902 (2016).
[8] S. S. Adler *et al.* (PHENIX Collaboration), Transverse-energy distributions at midrapidity in $p+p$, $d+{\rm Au}$, and ${\rm Au}+{\rm Au}$ collisions at $\sqrt{s_{NN}} = 62.4$–200 GeV and implications for particle-production models, Phys. Rev. C **89**, 044905 (2014).
[9] J. T. Mitchell, D. V. Perepelitsa, M. J. Tannenbaum, and P. W. Stankus, Tests of constituent-quark generation methods which maintain both the nucleon center of mass and the desired radial distribution in Monte Carlo Glauber models, Phys. Rev. C **93**, 054910 (2016).
[10] C. Loizides, Glauber modeling of high-energy nuclear collisions at the subnucleon level, Phys. Rev. C **94**, 024914 (2016).
[11] B. B. Back *et al.* (PHOBOS Collaboration), Scaling of charged particle production in $d+{\rm Au}$ collisions at $\sqrt{s_{NN}} = 200$ GeV, Phys. Rev. C **72**, 031901 (2005).
[12] C. Aidala *et al.* (PHENIX Collaboration), Measurements of azimuthal anisotropy and charged-particle multiplicity in $d+{\rm Au}$ collisions at $\sqrt{s_{NN}} = 200$, 62.4, 39, and 19.6 GeV, Phys. Rev. C **96**, 064905 (2017).

[13] S. Acharya *et al.* (ALICE Collaboration), Centrality and pseudorapidity dependence of the charged-particle multiplicity density in Xe-Xe collisions at $\sqrt{s_{\mathrm{NN}}} = 5.44$ TeV, arXiv:1805.04432.

[14] L. Adamczyk *et al.* (STAR Collaboration), Azimuthal Anisotropy in U + U and Au + Au Collisions at RHIC, Phys. Rev. Lett. **115**, 222301 (2015).

[15] A. Adare *et al.* (PHENIX Collaboration), Transverse energy production and charged-particle multiplicity at midrapidity in various systems from $\sqrt{s_{NN}} = 7.7$ to 200 GeV, Phys. Rev. C **93**, 024901 (2016).

[16] U. Heinz and R. Snellings, Collective flow and viscosity in relativistic heavy-ion collisions, Annu. Rev. Nucl. Part. Sci. **63**, 123 (2013).

[17] P. Romatschke and U. Romatschke, Relativistic fluid dynamics in and out of equilibrium: Ten years of progress in theory and numerical simulations of nuclear collisions, arXiv:1712.05815.

[18] J. L. Nagle and W. A. Zajc, Small system collectivity in relativistic hadron and nuclear collisions, Annu. Rev. Nucl. Part. Sci. **68**, 211 (2018).

[19] S. A. Voloshin and Y. Zhang, Flow study in relativistic nuclear collisions by Fourier expansion of azimuthal particle distributions, Z. Phys. C **70**, 665 (1996).

[20] B. B. Back *et al.* (PHOBOS Collaboration), Centrality and pseudorapidity dependence of elliptic flow for charged hadrons in Au + Au collisions at $\sqrt{s_{NN}} = 200$ GeV, Phys. Rev. C **72**, 051901 (2005).

[21] J. Adam *et al.* (ALICE Collaboration), Pseudorapidity dependence of the anisotropic flow of charged particles in Pb + Pb collisions at $\sqrt{s_{NN}} = 2.76$ TeV, Phys. Lett. B **762**, 376 (2016).

[22] G. Denicol, A. Monnai, and B. Schenke, Moving Forward to Constrain the Shear Viscosity of QCD Matter, Phys. Rev. Lett. **116**, 212301 (2016).

[23] M. Allen *et al.* (PHENIX Collaboration), PHENIX inner detectors, Nucl. Instrum. Methods Phys. Res., Sect. A **499**, 549 (2003).

[24] A. Adare *et al.* (PHENIX Collaboration), Centrality categorization for $R_{p(d)+A}$ in high-energy collisions, Phys. Rev. C **90**, 034902 (2014).

[25] K. Adcox *et al.* (PHENIX Collaboration), PHENIX central arm tracking detectors, Nucl. Instrum. Methods Phys. Res., Sect. A **499**, 489 (2003).

[26] C. Aidala *et al.*, The PHENIX forward silicon vertex detector, Nucl. Instrum. Methods Phys. Res., Sect. A **755**, 44 (2014).

[27] B. Alver *et al.* (PHOBOS Collaboration), PHOBOS results on charged particle multiplicity and pseudorapidity distributions in Au + Au, Cu + Cu, d + Au, and $p + p$ collisions at ultra-relativistic energies, Phys. Rev. C **83**, 024913 (2011).

[28] S. S. Adler *et al.* (PHENIX Collaboration), Measurement of Transverse Single-Spin Asymmetries for Midrapidity Production of Neutral Pions and Charged Hadrons in Polarized $p + p$ Collisions at $\sqrt{s} = 200$ GeV, Phys. Rev. Lett. **95**, 202001 (2005).

[29] S. S. Adler *et al.* (PHENIX Collaboration), J/ψ Production and Nuclear Effects for d + Au and $p + p$ Collisions at $\sqrt{s_{NN}} = 200$ GeV, Phys. Rev. Lett. **96**, 012304 (2006).

[30] P. Bozek and W. Broniowski, Transverse-momentum fluctuations in relativistic heavy-ion collisions from event-by-event viscous hydrodynamics, Phys. Rev. C **85**, 044910 (2012).

[31] P. Bozek, Flow and interferometry in 3 + 1-dimensional viscous hydrodynamics, Phys. Rev. C **85**, 034901 (2012).

[32] Z.-W. Lin, C. M. Ko, B.-A. Li, B. Zhang, and S. Pal, A multi-phase transport model for relativistic heavy ion collisions, Phys. Rev. C **72**, 064901 (2005).

[33] C. Aidala *et al.* (PHENIX Collaboration), Creating small circular, elliptical, and triangular droplets of quark-gluon plasma, arXiv:1805.02973.